Highly compact Proca stars with quartic self-interactions

Katsuki Aoki[1] and Masato Minamitsuji[2]

[1]*Center for Gravitational Physics and Quantum Information, Yukawa Institute for Theoretical Physics,
Kyoto University, 606-8502 Kyoto, Japan*
[2]*Centro de Astrofísica e Gravitação - CENTRA, Departamento de Física, Instituto Superior Técnico - IST,
Universidade de Lisboa - UL, Avenida Rovisco Pais 1, 1049-001 Lisboa, Portugal*

We study self-gravitating bound states of a complex vector field, known as Proca stars, with a new type of quartic-order self-interaction, which does not exist in the case of either a complex scalar field or a real vector field. Depending on the sign of the coupling constant, this quartic self-interaction can yield a distinct feature of Proca stars from the previously investigated self-interaction of the vector field. We find that self-gravitating solutions can be so compact that the photon sphere could form. However, we also show that the self-interaction gives rise to a ghost instability for the stars whose compactness is close that for the formation of a photon sphere, which might invalidate the formation of the photon sphere.

I. INTRODUCTION

While current experimental and observational data are consistent with the predictions of General Relativity (GR) [1,2], future observations of gravitational waves and those associated with the strong-field regime will provide us new opportunities to test the validity of GR [3–5]. The possibility of hypothetical horizonless compact objects [3–7] would also provide us to test the existence of the new particle sectors in the strong-field regime. Boson stars are the representative candidates of such compact objects [8–11] and are characterized by the Arnowitt-Deser-Misner (ADM) mass and Noether charge associated with the global $U(1)$ charge [12–14]. With an increase of the scalar amplitude, the ADM mass and Noether charge increase and the solutions below reaching the maximal values of them are dynamically stable [15–17]. Boson star solutions also exist in the presence of self-interacting potentials [9,18].

Boson star solutions can be naturally extended to the complex Proca field, which are known as Proca stars [19–25] (see also Ref. [26] for a Yang-Mills field and Refs. [27–29] for a spin-2 field). In the massive Proca theories, the properties of Proca stars are very similar to those of scalar boson stars [19], and have been extensively applied to astrophysics and gravitational-wave physics [30–35]. In the presence of the self-interaction potential of the complex Proca field $V(\bar{A}^\mu A_\mu)$, however, the situation is drastically modified. Proca star solutions cease to exist for the central Proca amplitude at a critical point [22–24]. The problem arises when the first radial derivative of the radial component of the Proca field diverges at a certain radius, beyond which one cannot integrate the field equations numerically. We have recently verified that the appearance of a singular point at a finite amplitude can be

interpreted as the onset of a gradient instability at the background level [36]. An independent but conceptually related problem is a ghost instability of a self-interacting Proca field [37–39] (see also Ref. [40]). Here, "ghost" and "gradient" instabilities are associated with the wrong signs of the kinetic and gradient terms in the Lagrangian, respectively. They grow arbitrarily fast if they continue existing in arbitrarily high-energy/-momentum scales, and the presence of these instabilities invalidates the perturbation theory within an infinitesimally short timescale. At the onset of a ghost or gradient instability, the hyperbolicity of equations of motion is lost. References [37–39] perform numerical simulations of the time evolution of a self-interacting real Proca field in different backgrounds and show that the time derivative of the temporal component of the Proca field diverges at a certain moment of time, beyond which one cannot follow the time evolution. The problem of a ghost instability is expected to be generic to the self-interacting Proca sector and independent of background geometries.

A ghost or gradient instability is indeed a pathology of the theory, if the self-interacting Proca field is a fundamental field. However, the self-interacting Proca theory could appear as a low-energy effective description of a more fundamental theory, and then ghost and gradient instability problems may be cured, once UV physics such as the dynamics of heavy fields is properly taken into consideration [36] (see also Refs. [25,26,41,42]). Reference [36] proposed a simple partial UV completion model of the self-interacting Proca theory with a new heavy scalar field. From the effective field theory (EFT) viewpoint, the onset of a gradient or ghost instability indicates a breakdown of the self-interacting Proca field as an EFT.

044045-1

It has been demonstrated that Proca star solutions, more precisely Proca-scalar star solutions as there is a scalar field in addition to the Proca field, continue to exist even beyond the critical point at which the EFT suffers from a gradient instability, and a small deviation is enough to regularize the singularity in the EFT. Several physical properties of the Proca-scalar star solutions (and nongravitating solutions) were studied by the authors of Ref. [43].[1] Then, it was shown that the maximal mass and compactness of Proca-scalar stars cannot exceed those of Proca stars in the pure Einstein-massive complex Proca theory, which is recovered in a certain limit from the UV theory, and the photon spheres and the innermost stable circular orbits cannot be formed in the stable branch.

Although Ref. [36] focused on the quartic-order self-interaction $(\bar{A}^{\mu} A_{\mu})^2$, analysis can be naturally extended to a more general self-interaction including higher-order terms of $\bar{A}^{\mu} A_{\mu}$. The issue on the existence of Proca stars provided one of the simplest setups that demonstrate a partial UV completion to cure the pathology of the self-interacting Proca field, in the sense that the system is given by a set of ordinary differential equations. While the problems of perturbations of the self-interacting Proca field on a non-trivial background [37–39] are formulated by a set of partial differential equations depending on both the space and time, they can be similarly resolved. Starting from an initial condition with a small amplitude where the EFT is valid, the system may evolve into a large amplitude of the vector field. Once UV physics is taken into account, the heavy mode should be excited before the breakdown of the EFT.

In the present paper, we will focus on another aspect of the self-interacting complex Proca field on the Proca star background while paying attention to UV physics. We will study properties of Proca stars in the presence of the new self-interaction of a complex Proca field A_{μ}, which includes the scalar product $\bar{A}^{\mu} \bar{A}^{\nu} A_{\mu} A_{\nu}$ [see Eq. (2.6) below] and vanishes in the limit of a real vector field. We will show that this new self-interaction could realize distinctive features of Proca stars, in comparison with those in the presence of the higher-order powers of $\bar{A}^{\mu} A_{\mu}$ explored in the literature [22–24]. We expect that, as in the case of the other theories, a possible ghost or gradient instability arises from the new self-interaction and they could also be cured by UV physics. Hence, we will concentrate on the properties of Proca stars in the regime of the EFT in the present paper. Yet, the underlying assumptions about UV physics lead to

nontrivial consequences on Proca stars, as we will discuss below.

This article is organized as follows. In Sec. II, we introduce the Einstein-complex Proca theory with the new self-interaction of a complex Proca field, which vanishes in the limit of a real Proca field. In Sec. III, we provide the basic equations to construct Proca star solutions. In Sec. IV, we discuss the properties of the Proca star solutions in our theory, especially focusing on the maximal compactness and the existence of a ghost or gradient instability. The last section, Sec. V, is devoted to giving a brief summary and conclusion.

II. SELF-INTERACTING COMPLEX PROCA FIELDS

Before initiating our analysis, it is instructive to mention differences among a complex scalar, a real vector field, and a complex vector field, to see how the vectorial and complex natures lead to the new interactions absent in the cases of the scalar field and the real vector field. Throughout the present paper, we will ignore derivative interactions, as they may be suppressed in low energies.

We first consider the following Lagrangian density of a complex scalar field Φ,

$$\mathcal{L}_{\Phi} = -\frac{1}{2} \nabla^{\mu} \bar{\Phi} \nabla_{\mu} \Phi - V_{\Phi}(\bar{\Phi}\Phi), \qquad (2.1)$$

where the overbar represents the complex conjugate, V_{Φ} is the potential, and ∇_{μ} denotes the covariant derivative associated with the spacetime metric $g_{\mu\nu}$. Note that here and in the rest the spacetime indices are raised by the inverse metric tensor $g^{\mu\nu}$, such as $\nabla^{\mu} = g^{\mu\nu} \nabla_{\nu}$, and lowered by the metric tensor $g_{\mu\nu}$. Since the Lagrangian density (2.1) must be real, the potential is a function of the modulus $\bar{\Phi}\Phi$. For instance, the potential up to the quartic order is given by $V_{\Phi}(\bar{\Phi}\Phi) = \frac{\mu_{\Phi}^2}{2} \bar{\Phi}\Phi + \frac{\lambda_{\Phi}}{4} (\bar{\Phi}\Phi)^2$, where μ_{Φ}^2 is the mass squared around the vacuum $\langle \Phi \rangle = 0$, which we shall assume positive. The coupling constant λ_{Φ} can be either positive or negative; a positive λ_{Φ} represents a repulsive self-interaction, while a negative λ_{Φ} leads to an attractive self-interaction.

We then consider a real vector field B_{μ} with the Lagrangian

$$\mathcal{L}_B = -\frac{1}{4} B^{\mu\nu} B_{\mu\nu} - V_B(B^{\mu} B_{\mu}), \qquad (2.2)$$

where $B_{\mu\nu} := \partial_{\mu} B_{\nu} - \partial_{\nu} B_{\mu}$. The potential $V_B(B^{\mu} B_{\mu})$ is a function of $B^{\mu} B_{\mu}$ since V_B should be a Lorentz-invariant scalar. Let us write it as $V_B(B^{\mu} B_{\mu}) = \frac{\mu_B^2}{2} B^{\mu} B_{\mu} + \frac{\lambda_B}{4} (B^{\mu} B_{\mu})^2$ up to the quartic order, which has a structure similar to the scalar potential V_{Φ}. Note that a self-interacting massive vector field is not UV complete on its own. Hence, Eq. (2.2)

---

[1]Reference [43] uses an Abelian-Higgs-like model as a partial UV completion of the quartic-order self-interaction. Note, however, that their model is different from the Abelian-Higgs model (see, e.g., Refs. [41,42]) because the vector field is complex rather than real. For instance, the field space of the scalar sector is no longer flat, differently from the Abelian-Higgs model (see, e.g., Eq. (4.10) of Ref. [36]).

should be regarded as a low-energy EFT, and a UV completion is needed when the theory loses its validity. The simplest example is the Higgs mechanism in which the self-interaction $(B^\mu B_\mu)^2$ arises as a result of integrating out the Higgs field. See, e.g., Refs. [25,26,36] in the context of boson stars. One may then notice that the sign of λ_B is necessarily negative [41,42] because it is determined by the squares of the coupling constant and the mass. The negative sign is not specific to the Higgs mechanism; it has to be negative for any (nongravitational) UV completion under the fundamental assumptions, namely unitarity, Poincaré invariance, causality, and locality, and the resultant bounds on low-energy EFTs are called positivity bounds [44]. It is, however, worth mentioning that the positivity bounds in gravitational systems are still subject to discussions and, especially, the sign of the Planck suppressed operators may depend on details of quantum gravity [45–51]. In the context of boson stars, the self-interactions are often supposed to be Planck suppressed [see Eq. (3.23) later], so it would be also interesting to investigate the positive value of λ_1 even though its UV completion is not known.

Now, we turn to our main focus, a complex vector field A_μ whose Lagrangian density is

$$\mathcal{L} = -\frac{1}{4}\bar{F}^{\mu\nu}F_{\mu\nu} - V, \qquad (2.3)$$

where $F_{\mu\nu} := \partial_\mu A_\nu - \partial_\nu A_\mu$, and the overbars again represent the complex conjugate. In the literature on Proca stars [19–26], the self-interacting potential V is often assumed to be a function of

$$Y := \bar{A}^\mu A_\mu \qquad (2.4)$$

just like the cases of a complex scalar field and a real vector field. However, there is the missing scalar invariant given by

$$Z := \bar{A}^\mu \bar{A}_\mu A^\nu A_\nu, \qquad (2.5)$$

which is independent from $(\bar{A}^\mu A_\mu)^2$, since A_μ has a spacetime index and is complex. Therefore, the most general potential up to the quartic order of A_μ and $\bar{A}_\mu$ is given by

$$V = \frac{\mu^2}{2}Y + \frac{\lambda_1}{4}Y^2 + \frac{\lambda_2}{4}(Z - Y^2), \qquad (2.6)$$

where μ is the mass of the Proca field and λ_1 and λ_2 are dimensionless self-coupling constants. The last term in Eq. (2.6) vanishes when A_μ is real, i.e., $\bar{A}_\mu = A_\mu$. As shown in the Appendix, the (nongravitational) positivity bounds conclude

$$\lambda_1 < 0, \qquad \lambda_2 < 0. \qquad (2.7)$$

The appearance of the second-type self-interaction from a Yang-Mills theory is well known, e.g., the self-interaction of the W boson, although the theory contains other vector fields in addition to the complex Proca field in this case. Nonrelativistic bosonic bound states in a Yang-Mills-Higgs system were found in Ref. [26] in which the self-interactions of the $SU(2)$ Yang-Mills field, i.e., three real vector fields, were studied. It should be, nevertheless, stressed that the bounds (2.7) are universal under the above-mentioned assumptions, regardless of whether A_μ is a part of a Yang-Mills field.

Therefore, there are two differences between the complex scalar field (scalar boson stars) and the complex vector field (Proca stars): the presence of the new self-interaction and the close connection between the sign of the coupling constants and UV physics. If the complex Proca field has the standard UV completion, the coupling constants must satisfy the inequalities (2.7) regardless of the details of UV completion. On the other hand, $\lambda_1 > 0$ or $\lambda_2 > 0$ requires unknown UV completion. The sign of the quartic order self-interaction of the Proca field has significant information about UV physics, and from the point of view of a bottom-up approach, the sign is determined through observations.

Having understood these distinctions, we study the properties of relativistic Proca star solutions in the Einstein-Proca theory

$$S = \int d^4x \sqrt{-g}\left[\frac{M_{\rm Pl}^2}{2}R - \frac{1}{4}\bar{F}^{\mu\nu}F_{\mu\nu} - V\right], \qquad (2.8)$$

where the Einstein-Hilbert term $(M_{\rm Pl}^2/2)R$ is added as the gravitational kinetic term to the self-interacting complex Proca field (2.3). Here, $M_{\rm Pl}$ is the reduced Planck mass, R represents the Ricci scalar associated with the metric $g_{\mu\nu}$, and V is given by Eq. (2.6).

Varying the action (2.8) with respect to $g_{\mu\nu}$, we obtain the gravitational equations of motion

$$M_{\rm Pl}^2 G_{\mu\nu} = T_{\mu\nu}, \qquad (2.9)$$

where we have defined the energy-momentum tensor of the complex Proca field

$$\begin{aligned} T_{\mu\nu} &= F_{(\mu}{}^\alpha \bar{F}_{\nu)\alpha} - \frac{1}{4}g_{\mu\nu}\bar{F}^{\rho\sigma}\bar{F}_{\rho\sigma} - Vg_{\mu\nu} \\ &\quad + [\mu^2 + (\lambda_1 - \lambda_2)Y]A_{(\mu}\bar{A}_{\nu)} \\ &\quad + \frac{\lambda_2}{2}(\bar{A}_\mu \bar{A}_\nu A^\rho A_\rho + A_\mu A_\nu \bar{A}^\rho \bar{A}_\rho). \end{aligned} \qquad (2.10)$$

Varying the action (2.8) with respect to $\bar{A}^\nu$, we obtain the Proca equation of motion

$$\nabla_\mu F^{\mu\nu} - [(\mu^2 + \lambda_1 A_\rho \bar{A}^\rho)A^\nu + \lambda_2 A^\rho(-\bar{A}_\rho A^\nu + A_\rho \bar{A}^\nu)] = 0. \qquad (2.11)$$

Acting ∇_ν on Eq. (2.11), we obtain the constraint condition

$$\nabla_\nu[(\mu^2 + \lambda_1 A_\rho \bar{A}^\rho)A^\nu + \lambda_2 A^\rho(-\bar{A}_\rho A^\nu + A_\rho \bar{A}^\nu)] = 0. \tag{2.12}$$

There exists the global $U(1)$ symmetry under the transformation $A_\mu \to e^{i\alpha}A_\mu$ with a constant α, and the associated Noether current is given by

$$j^\mu = \frac{i}{2}(\bar{F}^{\mu\nu}A_\nu - F^{\mu\nu}\bar{A}_\nu), \tag{2.13}$$

which satisfies the local conservation law $\nabla_\mu j^\mu = 0$.

III. PROCA STAR SOLUTIONS

A. Background equations

In this section, we present the basic equations to determine the structure of Proca star solutions in the theory (2.8) with Eq. (2.6). We assume the following ansatz for the metric and Proca fields,

$$g_{\mu\nu}dx^\mu dx^\nu = -\sigma(r)^2\left(1 - \frac{2m(r)}{r}\right)d\hat{t}^2$$
$$+ \left(1 - \frac{2m(r)}{r}\right)^{-1}dr^2 + r^2 d\Omega^2, \tag{3.1}$$

$$A_\mu dx^\mu = e^{-i\hat{\omega}\hat{t}}(a_0(r)dt + ia_1(r)dr), \tag{3.2}$$

where $\hat{t}$ and r are the temporal and radial coordinates, respectively; $\sigma(r)$, $m(r)$, $a_0(r)$, and $a_1(r)$ are the real functions of r; and $\hat{\omega}$ is the frequency which is determined under suitable boundary conditions. For a Proca star solution, the frequency $\hat{\omega}$ is real and positive, so the Proca field is stationary and neither grows nor decays in time. For a time-dependent complex Proca field, each component of the energy-momentum tensor (2.10) would in general become time dependent. However, we stress that the ansatz for the Proca field (3.2) is compatible with the staticity and spherical symmetry of the spacetime (3.1) because in each component of the energy-momentum tensor (2.10) the explicit time dependence $e^{-i\hat{\omega}\hat{t}}$ in A_μ and its derivative is canceled out by its complex conjugate $e^{i\hat{\omega}\hat{t}}$ in $\bar{A}_\mu$ and its derivative for the ansatz Eq. (3.2). Hence, the components of the energy-momentum tensor (2.10) do not contain the time dependence.

Substituting the above ansatz into the Einstein and Proca field equations, Eqs. (2.9) and (2.11), we find that $\sigma(r)$, $m(r)$, $a_0(r)$, and $a_1(r)$ obey the first-order ordinary differential equations

$$\frac{dm}{dr} = F_m[m(r), \sigma(r), a_0(r), a_1(r); r], \tag{3.3}$$

$$\frac{d\sigma}{dr} = F_\sigma[m(r), \sigma(r), a_0(r), a_1(r); r], \tag{3.4}$$

$$\frac{da_0}{dr} = F_0[m(r), \sigma(r), a_0(r), a_1(r); r], \tag{3.5}$$

$$\frac{da_1}{dr} = F_1[m(r), \sigma(r), a_0(r), a_1(r); r], \tag{3.6}$$

where

$$F_m := \frac{1}{8M_{\rm Pl}^2}\left[2r\mu^2 a_1^2(r - 2m) + 4a_1^2(r\mu^2 + \lambda_1 a_1^2(r - 2m))(r - 2m) + \lambda_1 a_1^4(r - 2m)^2 - \frac{2r^2\hat{\omega}^2 a_1^2}{\sigma^2} - \frac{2r^2(\lambda_1 - 2\lambda_2)a_0^2 a_1^2}{\sigma^2}\right.$$
$$\left. - \frac{r^2}{\sigma^4}\left[\frac{3r^2\lambda_1 a_0^4}{(r - 2m)^2} - \frac{2r\mu^2 a_0^2\sigma^2}{r - 2m} - \frac{2a_1^2\sigma^2}{\hat{\omega}^2}\left\{\hat{\omega}^2 + (\lambda_1 - 2\lambda_2)a_0^2 - \frac{(r\mu^2 + \lambda_1 a_1^2(r - 2m))(r - 2m)\sigma^2}{r^2}\right\}^2\right]\right], \tag{3.7}$$

$$F_\sigma := -\frac{1}{2M_{\rm Pl}^2}\left[\frac{r^4\lambda_1 a_0^4}{(r - 2m)^3\sigma^3} - \frac{r^3\mu^2 a_0^2}{(r - 2m)^2\sigma}\right.$$
$$\left. - a_1^2(r\mu^2 + \lambda_1 a_1^2(r - 2m))\sigma\right], \tag{3.8}$$

$$F_0 := \frac{a_1}{\hat{\omega}}\left(\hat{\omega}^2 + (\lambda_1 - 2\lambda_2)a_0^2\right.$$
$$\left. - \frac{\sigma^2(r\mu^2 + \lambda_1 a_1^2(r - 2m))(r - 2m)}{r^2}\right), \tag{3.9}$$

and F_1 is a complicated function of (m, σ, a_0, a_1), which contains

$$\mathcal{H}(r) := -r^2(\lambda_1 - 2\lambda_2)a_0^2 + (r\mu^2 + 3\lambda_1 a_1^2(r - 2m))$$
$$\times (r - 2m)\sigma^2 \tag{3.10}$$

in the denominator. In integrating Eqs. (3.3)–(3.6), in case one hits the point where $\mathcal{H}(r) = 0$, one cannot integrate them beyond this point, and hence there is no Proca star solution. As we will see later, the appearance of the point $\mathcal{H}(r) = 0$ can be interpreted as the onset of a gradient instability at the background level [36].

Solving Eqs. (3.3)–(3.6) in the vicinity of the center $r = 0$, the regular solution can be obtained as

$$m(r) = \frac{f_0^2(-3f_0^2\lambda_1 + 2\mu^2\sigma_0^2)}{24M_{\rm Pl}^2\sigma_0^4}r^3 + \mathcal{O}(r^4), \tag{3.11}$$

$$\sigma(r) = \sigma_0 + \frac{f_0^2(-f_0^2\lambda_1 + \mu^2\sigma_0^2)}{4M_{\mathrm{Pl}}^2\sigma_0^3}r^2 + \mathcal{O}(r^4), \qquad (3.12)$$

$$a_0(r) = f_0$$
$$- \frac{f_0(f_0^2\lambda_1 - \mu^2\sigma_0^2)(f_0^2(\lambda_1 - 2\lambda_2) - \mu^2\sigma_0^2 + \hat{\omega}^2)}{6f_0^2(\lambda_1 - 2\lambda_2)\sigma_0^2 - 6\mu^2\sigma_0^4}r^2$$
$$+ \mathcal{O}(r^4), \qquad (3.13)$$

$$a_1(r) = -\frac{f_0\hat{\omega}(f_0^2\lambda_1 - \mu^2\sigma_0^2)}{3\sigma_0^2 f_0^2(\lambda_1 - 2\lambda_2) - 3\mu^2\sigma_0^4}r + \mathcal{O}(r^3). \quad (3.14)$$

Under the regular boundary conditions (3.11)–(3.14) near the origin $r = 0$, we numerically integrate Eqs. (3.3)–(3.6) toward infinity. For a given set of parameters, if we choose $\hat{\omega}$ to be a proper value, m and σ exponentially approach constant values, $m_\infty > 0$ and $\sigma_\infty > \sigma_0 > 0$, respectively, and a_0 and a_1 exponentially approach zero as $e^{-\sqrt{\mu^2-\omega^2}r}$, where the proper frequency for the observer sitting at the infinity $r \to \infty$ is defined by

$$\omega := \frac{\hat{\omega}}{\sigma_\infty}. \qquad (3.15)$$

The exponential falloff of the Proca field in the large distance limit as $e^{-\sqrt{\mu^2-\omega^2}r}$ requires

$$\omega < \mu. \qquad (3.16)$$

Thus, as $r \to \infty$, the metric exponentially approaches the Schwarzschild form

$$ds^2 \to -\sigma_\infty^2\left(1 - \frac{2m_\infty}{r}\right)d\hat{t}^2 + \left(1 - \frac{2m_\infty}{r}\right)^{-1}dr^2 + r^2 d\Omega_2^2, \qquad (3.17)$$

where the proper time measured by the observer at $r = \infty$ is given by $t = \sigma_\infty \hat{t}$. In the limit $f_0 \to 0$, $\omega \to \mu$, the Proca field profiles $a_0(r)$ and $a_1(r)$ trivially vanish, and the Minkowski solution is obtained. Note that there can be multiple solutions satisfying the same boundary conditions near the origin and in the large distance region for discrete eigenvalues of ω, for a given set of the parameters. In this paper, we will focus only on ground state solutions obtained for the lowest eigenvalue of ω, where $a_0(r)$ and $a_1(r)$ have one and zero nodes, respectively (see Fig. 1).

There are several conserved charges that characterize the properties of Proca stars. The first is the ADM mass

$$M := 8\pi M_{\mathrm{Pl}}^2 m_\infty, \qquad (3.18)$$

which is determined by the asymptotic value of the mass function $m(r)$. The second is the Noether charge associated
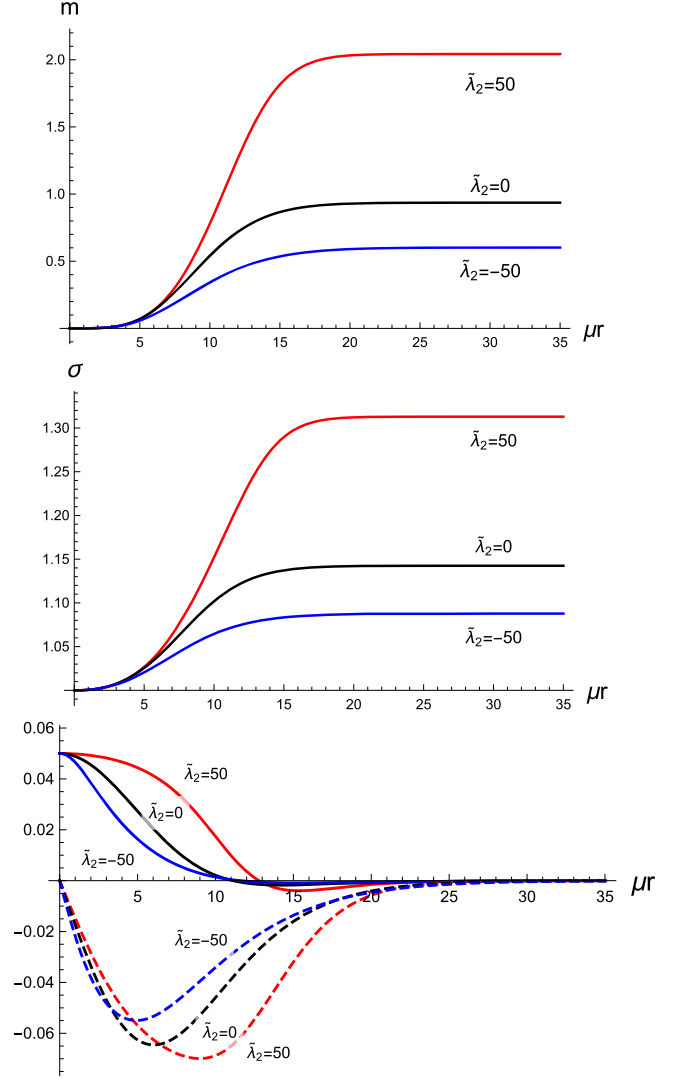

FIG. 1. The profiles of the metric functions m (top), σ (middle), and the Proca field (bottom) for Proca star solutions in the ground state are shown as the functions of μr for $f_0 = 0.05$ with the specified coupling constants. In the bottom panel, the solid and dashed curves correspond to the profiles $a_0(r)$ and $a_1(r)$, respectively. Note that the dimensionless coupling constant $\tilde{\lambda}_2$ is defined in Eq. (3.23).

with the global $U(1)$ symmetry, which is given by integrating $j^{\hat{t}}$ in Eq. (2.13) over a constant-$\hat{t}$ hypersurface,

$$Q := \int_\Sigma d^3x\sqrt{-g}j^{\hat{t}} = \int_0^\infty dr\frac{4\pi r^2 a_1(\hat{\omega}a_1 - a_0')}{\sigma}, \qquad (3.19)$$

where Σ denotes a constant time hypersurface. Q physically describes the particle number of the Proca field, and the Proca star is gravitationally bound, when

$$\mu Q - M > 0. \qquad (3.20)$$

In the case of Proca stars as well as boson stars, there is no unique definition of the radius, and so we need to

introduce an effective radius which characterizes the size of the distribution of the Proca field. First, we define the radius $\mathcal{R}_{95}$ by

$$m(\mathcal{R}_{95}) = 0.95 \times m_\infty, \tag{3.21}$$

at which the mass function $m(r)$ reaches 95% of the ADM mass [see Eq. (3.18) for the relation of M and m_∞]. We also introduce the radius normalized by Q [9]

$$\mathcal{R} := \frac{1}{Q} \int_\Sigma d^3 x \sqrt{-g}(r\hat{j}^i) = \frac{4\pi}{Q} \int_0^\infty dr \frac{r^3 a_1(\hat{\omega} a_1 - a_0')}{\sigma}. \tag{3.22}$$

While $\mathcal{R}_{95}$ can be interpreted as an astronomical surface of a Proca star within which the most energy of the Proca field is confined, $\mathcal{R}$ can be interpreted as the expectation value of the radius that characterizes the distribution of the Proca field. We will numerically find $\mathcal{R}_{95} > \mathcal{R}$ in a typical Proca star solution.

By introducing the rescaled dimensionless quantities by

$$\tilde{\omega} := \frac{\hat{\omega}}{\mu}, \qquad \tilde{r} := r\mu, \qquad \tilde{m} := \mu m,$$

$$\tilde{a}_0 := \frac{a_0}{M_{\rm Pl}}, \qquad \tilde{a}_1 := \frac{a_1}{M_{\rm Pl}}, \qquad \tilde{\lambda}_{1,2} := \frac{M_{\rm Pl}^2 \lambda_{1,2}}{\mu^2}, \tag{3.23}$$

the evolution equations (3.3)–(3.6) can be rewritten into the form without the dimensionful quantities μ and $M_{\rm Pl}$. Thus, without loss of generality, for the numerical analysis, we set $\mu = M_{\rm Pl} = 1$, and if necessary, it is straightforward to give back the dependence on μ and $M_{\rm Pl}$. In addition, as σ_0 corresponds to the freedom of the rescaling of the time coordinate, without loss of generality, we may also set $\sigma_0 = 1$. Therefore, only the remaining physical parameters are f_0, λ_1, and λ_2.

Proca star solutions have been constructed for the self-interacting potential with $\lambda_1 \neq 0$ and $\lambda_2 = 0$ in Refs. [22–24]. Instead, in this work, we will focus on the interaction $Z - Y^2$, which vanishes in the case of the real Proca field, and hence consider the case of

$$\lambda_1 = 0, \qquad \lambda_2 \neq 0. \tag{3.24}$$

Clearly, the most general case is that of $(\lambda_1 \neq 0, \lambda_2 \neq 0)$. However, as far as we investigated several choices of $(\lambda_1 \neq 0, \lambda_2 \neq 0)$, the physical properties of Proca stars such as the mass-radius relation for the general case can be simply understood by a combination of the two opposite cases, i.e., $(\lambda_2 \neq 0, \lambda_1 = 0)$ and $(\lambda_1 \neq 0, \lambda_2 = 0)$. Thus, in this paper, we focus on the case (3.24) and its difference from the opposite case $(\lambda_1 \neq 0, \lambda_2 = 0)$ discussed in Refs. [22–24].

In Fig. 1, the profiles of the metric function m (top), the metric function σ (middle), and the Proca field (bottom) for Proca star solutions in the ground state are shown as the functions of μr for $f_0 = 0.05$. The top and middle panels represent the profiles of $m(r)$ and $\sigma(r)$, while the solid and dashed curves in the lower panel correspond to the profiles of $a_0(r)$ and $a_1(r)$, respectively. The top and middle panels show that both the metric functions $m(r)$ and $\sigma(r)$ approach larger/smaller constant positive values in the large distance regime $r\mu \gg 1$ for positive/negative values of λ_2, than those for $\lambda_2 = 0$. The bottom panel shows that the profiles of the Proca field are more broadened in the vicinity of the center of the star for positive values of λ_2 and more compressed for negative values of λ_2. We note that the profiles of $\tilde{\alpha}_0(r)$ and $\tilde{\alpha}_1(r)$, which will be defined in Eq. (3.37), are almost identical to $a_0(r)$ and $a_1(r)$ in Fig. 1. As for Proca star solutions in other theories [19–25], the temporal component of the complex Proca field $a_0(r)$ in the ground state crosses zero once and hence has a single node, which is in contrast with the case of scalar boson stars in the ground state where the radial profile of the complex scalar field has zero nodes.

B. Effective metric for the Proca field perturbations

On top of Proca star solutions, we consider small perturbations of the complex Proca field. As is well known, the propagations of the longitudinal modes of A_μ are modified by the self-interactions, and a ghost or gradient instability may appear around a nontrivial background configuration of A_μ. In this subsection, we study a high-frequency limit of the perturbations around a nontrivial background and find the effective metric on which the perturbations propagate. A ghost (or gradient) instability appears when the signature of the temporal (or radial) component of the effective metric changes.

We perturb these equations around a nontrivial background of A_μ and pick up the highest derivative terms which characterize the propagation of the Proca field in the high-frequency limit. The background is denoted by the same symbol A_μ, while the perturbations are given by $\delta A_\mu + \partial_\mu \pi$, where π is the Stückelberg field representing the longitudinal modes. One can easily find that Eq. (2.11) is reduced to the standard Maxwell equation in the high-frequency limit,

$$\partial^2 \delta A_\mu - \partial^\nu \partial_\mu \delta A_\nu + \cdots = 0, \tag{3.25}$$

where $\cdots$ are the terms that are at most linear in derivatives of the perturbations. On the other hand, the perturbed equation of (2.12) takes the form

$$K^{\mu\nu} \partial_\mu \partial_\nu \begin{pmatrix} \pi^1 \\ \pi^2 \end{pmatrix} + \cdots = 0, \tag{3.26}$$

where π^1 and π^2 are the real and imaginary parts of π, and the components of the 2×2 matrix $\boldsymbol{K}^{\mu\nu}$ are given by

$$(\boldsymbol{K}^{\mu\nu})_{11} = \left(\frac{\mu^2}{2} + \frac{\lambda_1}{2}Y - \lambda_2 A^{2\alpha}A_\alpha^2\right)g^{\mu\nu}$$
$$+ \lambda_1 A^{1\mu}A^{1\mu} + \lambda_2 A^{2\mu}A^{2\nu}, \qquad (3.27)$$

$$(\boldsymbol{K}^{\mu\nu})_{12} = (\boldsymbol{K}^{\mu\nu})_{21} = \lambda_1 - \lambda_2 A^{1(\mu}A^{2\nu)} + \lambda_2(A^{1\alpha}A_\alpha^2)g^{\mu\nu}, \qquad (3.28)$$

$$(\boldsymbol{K}^{\mu\nu})_{22} = \left(\frac{\mu^2}{2} + \frac{\lambda_1}{2}Y - \lambda_2 A^{1\alpha}A_\alpha^1\right)g^{\mu\nu} + \lambda_1 A^{2\mu}A^{2\mu} + \lambda_2 A^{1\mu}A^{1\nu} \qquad (3.29)$$

with $A_\mu = A_\mu^1 + iA_\mu^2$. Here, the covariant derivatives are replaced with the partial ones because we are focusing on the short wavelength in comparison with the background spacetime curvature scale. The dispersion relation of the longitudinal modes is given by a root of

$$\det(\boldsymbol{K}^{\mu\nu}k_\mu k_\nu) = 0 \qquad (3.30)$$

with k_μ being a four-wave-vector.

Either when $\lambda_1 = 0$ or $\lambda_2 = 0$, the dispersion relation (3.30) is factorized,

$$\det(\boldsymbol{K}^{\mu\nu}k_\mu k_\nu) \propto k^2 \times g_{\text{eff}}^{\mu\nu}k_\mu k_\nu = 0 \quad \text{(when } \lambda_1\lambda_2 = 0\text{)}; \qquad (3.31)$$

that is, one of the longitudinal modes propagates on the light cone of the spacetime metric, while the other propagates on the effective metric $g_{\text{eff}}^{\mu\nu}$. In the following, let us concentrate on the case $\lambda_1 = 0$, which is our main interest in the present paper. The effective metric with $\lambda_1 = 0$ is given by

$$g_{\text{eff}}^{\mu\nu} = g^{\mu\nu}[(1 - \lambda_2 Y/\mu^2)^2 - \lambda_2^2 Z/\mu^4]$$
$$+ 2A^{(\mu}\bar{A}^{\nu)}(\lambda_2/\mu^2 - \lambda_2^2 Y/\mu^4)$$
$$+ \frac{\lambda_2^2}{\mu^4}(A^\alpha A_\alpha \bar{A}^\mu \bar{A}^\nu + \bar{A}^\alpha \bar{A}_\alpha A^\mu A^\nu) \qquad (3.32)$$

of which the determinant is given by

$$\det(g_{\text{eff}}^{\mu\nu}) = \det(g^{\mu\nu})[(1 - \lambda_2 Y/\mu^2)^2 - \lambda_2^2 Z/\mu^4]^3. \qquad (3.33)$$

In particular, the nonvanishing components of $\mathcal{H}^\mu_{\ \nu} := g_{\text{eff}}^{\mu\alpha}g_{\alpha\nu}$ under the spherically symmetric ansatz are

$$\mathcal{H}^t_{\ t} = 1 - 2\tilde{\lambda}_2\tilde{\alpha}_1^2, \qquad (3.34)$$

$$\mathcal{H}^r_{\ r} = 1 + 2\tilde{\lambda}_2\tilde{\alpha}_0^2, \qquad (3.35)$$

$$\mathcal{H}^\theta_{\ \theta} = \mathcal{H}^\varphi_{\ \varphi} = (1 - 2\tilde{\lambda}_2\tilde{\alpha}_1^2)(1 + 2\tilde{\lambda}_2\tilde{\alpha}_0^2), \qquad (3.36)$$

where

$$\tilde{\alpha}_0 := \frac{\tilde{a}_0}{\sigma(1 - 2m/r)^{1/2}}, \qquad \tilde{\alpha}_1 := \tilde{a}_1(1 - 2m/r)^{1/2}. \qquad (3.37)$$

A ghost or gradient instability occurs at a point where $\mathcal{H}^t_{\ t} = 0$ or $\mathcal{H}^r_{\ r} = 0$, respectively. In the case of $\lambda_1 = 0$,

$$\mathcal{H}(r) = r\mu^2(r - 2m)\sigma^2\mathcal{H}^r_{\ r}, \qquad (3.38)$$

where $\mathcal{H}(r)$ is defined in Eq. (3.10). Thus, a gradient instability occurs at the point $\mathcal{H} = 0$, where the background static solution to the equations (3.3)–(3.6) ceases to exist. Note that the condition to have a singular effective metric, $(1 - \lambda_2 Y/\mu^2)^2 - \lambda_2^2 Z/\mu^4 = \mathcal{H}^t_{\ t}\mathcal{H}^r_{\ r} = 0$, is expressed by coordinate-invariant scalar quantities, meaning that the singularity is not a coordinate singularity.

In the case $\lambda_2 < 0$, $\mathcal{H}^t_{\ t} > 0$ always, but $\mathcal{H}^r_{\ r}$ may change the sign, and hence a gradient instability could occur. As we have shown in Fig. 1, the function a_0 takes the maximum value at $r = 0$ and approaches zero as $r \to \infty$. The normalized function $\tilde{\alpha}_0$ also shows a qualitatively similar behavior. Hence, $\mathcal{H}^r_{\ r}$ should take the minimum value at $r = 0$ for $\lambda_2 < 0$ and whether $\mathcal{H}^r_{\ r}$ crosses zero or not can be checked by the sign of the central value of $\mathcal{H}^r_{\ r}$. Using Eqs. (3.11)–(3.14), in the vicinity of the center $r = 0$, $\mathcal{H}^r_{\ r}$ can be expanded as

$$\mathcal{H}^r_{\ r}(r \to 0) \to 1 + \frac{2\lambda_2 f_0^2}{\mu^2\sigma_0^2}. \qquad (3.39)$$

Therefore, $\mathcal{H}^r_{\ r}$ does not cross zero for

$$f_0 < \frac{\mu\sigma_0}{\sqrt{2|\lambda_2|}}, \qquad (3.40)$$

while $\mathcal{H}^r_{\ r}$ changes the sign if the central amplitude f_0 exceeds the critical value. In other words, Proca star solutions can be constructed numerically only for f_0 satisfying Eq. (3.40). If one wants to find solutions beyond the critical point, one needs to include the effects of UV physics [36].

In the case $\lambda_2 > 0$, $\mathcal{H}^r_{\ r} > 0$ always, but $\mathcal{H}^t_{\ t}$ may change the sign, and hence a ghost instability could occur. As we will see later, for $\lambda_2 > 0$, a ghost instability appears for a sufficiently large central amplitude. However, the point at which a ghost instability appears is neither the vicinity of the center nor the large distance regime because $\tilde{a}_1^2$ (or $\tilde{\alpha}_1^2$) takes the maximum value at a finite distance as shown in Fig. 1. The critical amplitude cannot be estimated analytically, and the critical amplitude will be obtained numerically in the next section.

IV. PROPERTIES OF PROCA STARS

In this section, we construct Proca star solutions numerically. As mentioned in Sec. III, for the numerical analysis, we set $M_{\rm Pl} = \mu = 1$ and $\sigma_0 = 1$. After constructing the solutions, we shall give back the dependence on $M_{\rm Pl}$ and μ properly.

Since typically μ is assumed to be much smaller than the Planck mass $M_{\rm Pl}$, the values of $|\tilde{\lambda}_i|$ $(i = 1, 2)$ given by Eq. (3.23) can be much larger than unity. Hence, $|\tilde{\lambda}_i| = \mathcal{O}(1)$ corresponds to the case with the Planck suppressed self-interactions, and $|\tilde{\lambda}_i| \gg \mathcal{O}(1)$ may be interpreted as the case when the cutoff of the EFT is below $M_{\rm Pl}$ (but still above μ). Note that in $M_{\rm Pl} = 1$ and $\mu = 1$, $\tilde{\lambda}_i = \lambda_i$.

A. $M-\omega$ and $Q-\omega$ relations

1. $\lambda_2 < 0$ ($\tilde{\lambda}_2 < 0$)

In Fig. 2, M (solid curves) and μQ (dashed curves) are shown as the functions of ω/μ for $\tilde{\lambda}_2 = 0$ (black), -10 (green), -20 (blue), and -50 (red) from the top to the bottom. M and μQ are shown in the units of $8\pi M_{\rm Pl}^2/\mu$. The curves for $\lambda_2 < 0$ are terminated at the amplitude saturating the bound (3.40), above which we cannot numerically construct Proca star solutions. As argued in Ref. [36], the onset of a gradient instability may not be an intrinsic pathology of the self-interacting Proca theories but may be interpreted as the breakdown of the description of the Einstein-Proca theory (2.8) as a low-energy EFT. For $\lambda_2 < 0$, both M and μQ are suppressed, and Proca star solutions exist only for the frequency ω relatively close to μ. Proca stars are gravitationally bound $\mu Q > M$. Similarly to the conventional case $\tilde{\lambda}_2 = 0$, the values of M and μQ do not differ so significantly. The $M-\omega$ and $Q-\omega$ relations with $\lambda_2 < 0$ are qualitatively similar to the Proca stars with the self-interaction $\lambda_1 < 0$ [22].
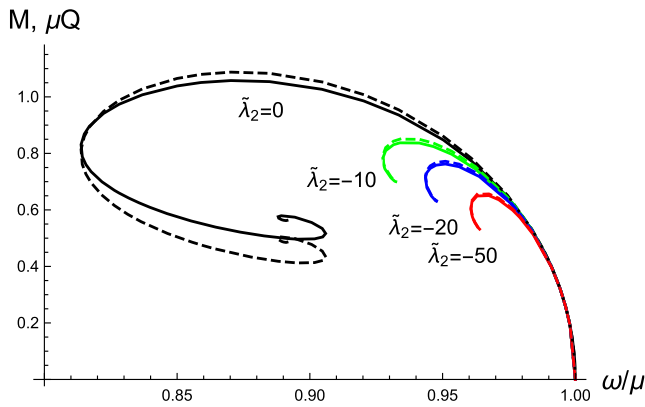
2. $\lambda_2 > 0$ ($\tilde{\lambda}_2 > 0$)

Let us then consider the positive value of λ_2. In Fig. 3, M (solid curves) and μQ (dashed curves) are shown as the functions of ω/μ for $\tilde{\lambda}_2 = 0$ (black), 1 (green), 10 (blue), 50 (orange), and 200 (red) from the bottom to the top. M and μQ are shown in the units of $8\pi M_{\rm Pl}^2/\mu$. For $\lambda_2 > 0$, we find that the self-interaction significantly enhances both M and μQ. However, unlike the conventional case, the value of μQ is more enhanced than M, and then the $M - \omega$ relation is no longer close to the $Q - \omega$ relation for a large value of $\tilde{\lambda}_2$. In particular, we find that Eq. (3.20) is satisfied even in the second branch of Proca stars, i.e., after reaching the minimum value of the frequency ω, implying that Proca stars are gravitationally bound.

For $\tilde{\lambda}_2 > \mathcal{O}(20)$, we find solutions that the temporal component of the effective metric changes the sign at an intermediate radius. We show several profiles of $\mathcal{H}^t{}_t$ with different central amplitudes of the vector field for $\tilde{\lambda}_2 = 50$ in Fig. 4. As the central amplitude increases, the minimum value of $\mathcal{H}^t{}_t$ decreases, and nodes of $\mathcal{H}^t{}_t = 0$ appear beyond a critical point. Proca star solutions then suffer from a ghost instability, which should invalidate the EFT description. On the other hand, the minimum value of $\mathcal{H}^t{}_t$ starts to increase if the central amplitude further increases, and then the nodes disappear. These critical points are shown in the circles and the squares in Fig. 3, respectively. A negative region of $\mathcal{H}^t{}_t$ exists in solutions between the circle and the square. For $\tilde{\lambda}_2 = 200$, the profiles of $\mathcal{H}^t{}_t$ are qualitatively similar, and a negative region of $\mathcal{H}^t{}_t$ appears beyond a critical point as indicated by the circles in Fig. 3. However, we numerically find that $\mathcal{H}^t{}_t$ still has a negative region, even if the central amplitude further increases, differently from the case of $\tilde{\lambda}_2 = 50$.
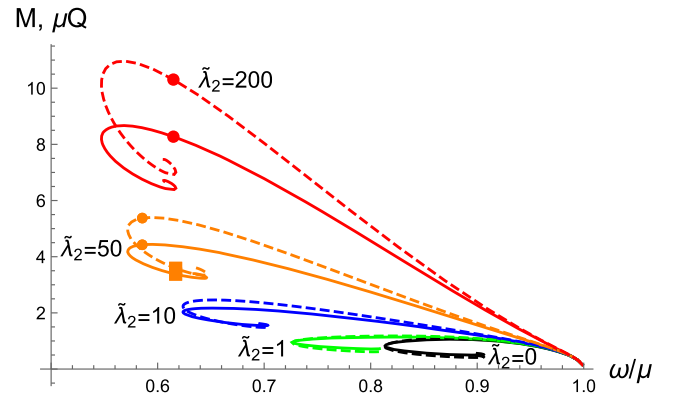

FIG. 2. M (solid curves) and μQ (dashed curves) are shown as the functions of ω/μ for $\tilde{\lambda}_2 = 0$ (black), -10 (green), -20 (blue), and -50 (red) from the top to the bottom. M and μQ are shown in the units of $8\pi M_{\rm Pl}^2/\mu$.

FIG. 3. M (solid curves) and μQ (dashed curves) are shown as the functions of ω/μ for $\tilde{\lambda}_2 = 0$ (black), 1 (green), 10 (blue), 50 (orange), and 200 (red) from the bottom to the top. M and μQ are shown in the units of $8\pi M_{\rm Pl}^2/\mu$. For $\tilde{\lambda}_2 = 50$ and 200, the points indicate the critical points beyond which a negative region of $\mathcal{H}^t{}_t$ appears (circles) and disappears (square).
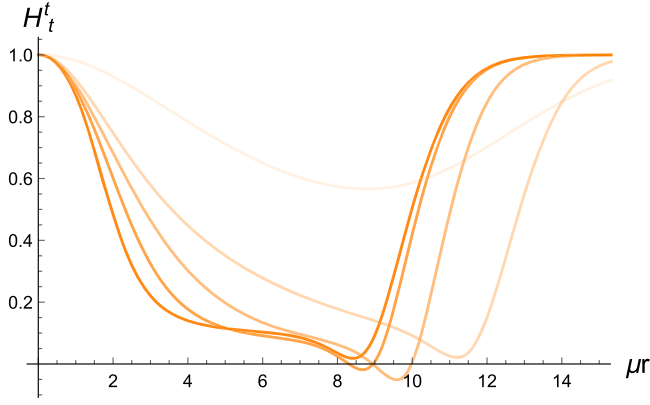
FIG. 4. Profiles of the temporal component of the effective metric $\mathcal{H}^t{}_t$ for $\tilde{\lambda}_2 = 50$. A deeper color corresponds to a larger central amplitude of the Proca field.

B. Mass-radius relations

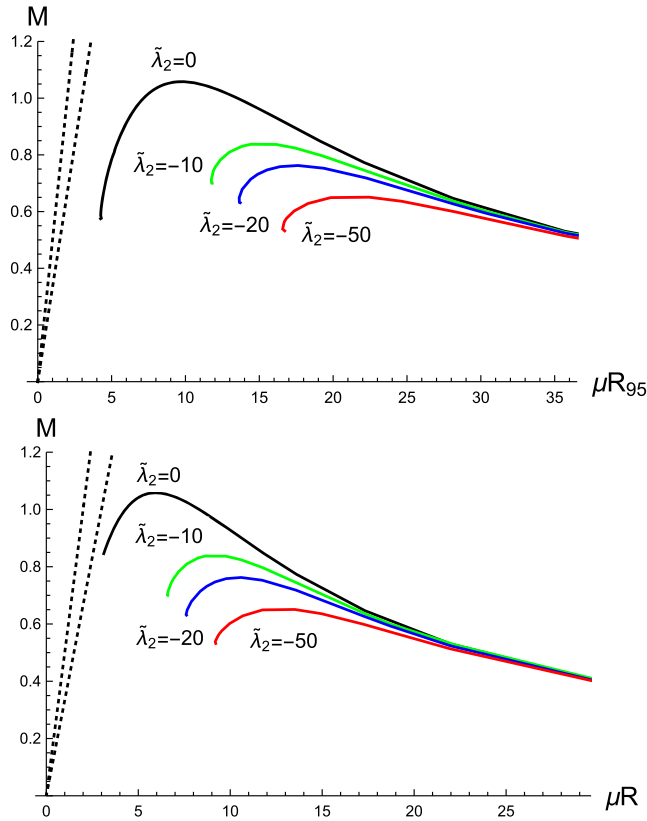### 1. $\lambda_2 < 0$ ($\tilde{\lambda}_2 < 0$)

In the top and bottom panels of Fig. 5, M is shown as the functions of $\mu\mathcal{R}_{95}$ (top) and $\mu\mathcal{R}$ (bottom) for $\tilde{\lambda}_2 = 0$ (black), -10 (green), -20 (blue), and -50 (red) [see

FIG. 5. M is shown as the function of $\mu\mathcal{R}_{95}$ (top) and $\mu\mathcal{R}$ (bottom) for $\tilde{\lambda}_2 = 0$ (black), -10 (green), -20 (blue), and -50 (red), respectively. The dotted lines from the top have the tilts $1/2$ and $1/3$, respectively. M is shown in the units of $8\pi M_{\mathrm{Pl}}^2/\mu$.

Eqs. (3.21) and (3.22)]. The dotted lines from the top have the tilts $1/2$ and $1/3$. Crossing these lines may indicate the formation of an event horizon and a photon sphere, respectively. As mentioned in Sec. III A, although there is no unique definition of the surface of a Proca star, $\mathcal{R}_{95}$ should be more suitable to characterize it, because $\mathcal{R}_{95}$ encloses the most of the volume where the energy of the Proca field is contained, especially for a Proca star with a more localized profile of the Proca field. Thus, crossing the dashed line $M = \mathcal{R}_{95}/3$ strongly indicates the formation of a photon sphere. M is shown in the units of $8\pi M_{\mathrm{Pl}}^2/\mu$. We find $\mathcal{R}_{95} > \mathcal{R}$ as mentioned previously. The relative difference between $\mathcal{R}_{95}$ and $\mathcal{R}$ is about 60% for the least compact stars and exceeds 80% for the most compact stars. In comparison with the case of $\tilde{\lambda}_2 = 0$, M is always suppressed, and hence Proca stars become less compact than the conventional case of $\tilde{\lambda}_2 = 0$. Note that the other self-interaction $(\bar{A}^\mu A_\mu)^2$ with $\lambda_1 < 0$ also leads to a similar effect, making Proca stars less compact. In other words, observationally, it would be difficult to distinguish Proca star solutions for $\lambda_2 < 0$ from those in other theories.

2. $\lambda_2 > 0$ ($\tilde{\lambda}_2 > 0$)

Opposite to the case with $\lambda_2 < 0$, the self-interaction with $\lambda_2 > 0$ gives compact Proca stars. In Fig. 6, M is shown as the function of $\mathcal{R}_{95}$ (top) and $\mathcal{R}$ (bottom) for $\tilde{\lambda}_2 = 0$ (black), 1 (green), 10 (blue), 50 (orange), and 200 (red) in the units of $8\pi M_{\mathrm{Pl}}^2/\mu$. The dotted lines from the top represent those with the tilts $1/2$ and $1/3$. For a sufficiently large $\tilde{\lambda}_2$, the mass-radius relation can exceed the line $M = \mathcal{R}_{95}/3$, suggesting a formation of the photon sphere. However, for $\tilde{\lambda}_2 = 50$ and 200, the solutions with large amplitudes of the Proca field are suffered from a ghost instability, and the critical points appear in the vicinity of the line $M = \mathcal{R}_{95}/3$. In particular, in the case of $\tilde{\lambda}_2 = 50$, both critical points (the circle and the square) are situated in the vicinity of the line $M = \mathcal{R}_{95}/3$, and the solutions have a negative region of $\mathcal{H}^t{}_t$ only in $M \gtrsim \mathcal{R}_{95}/3$. On the other hand, the curves for $\tilde{\lambda}_2 = 0$, 1, 10 are free from a ghost instability but are always below the line $M = \mathcal{R}_{95}/3$. Therefore, a ghost instability somehow forbids the formation of a photon sphere at least within the regime of validity of the EFT. We need a UV completion to properly discuss the properties of the Proca stars with $M \gtrsim \mathcal{R}_{95}/3$.

The bottom one of Fig. 6 shows the mass-radius relation by using the effective radius defined by (3.22) or the reference. We always find that $\mathcal{R} < \mathcal{R}_{95}$, and the curves for $\lambda_2 > 0$ can cross the line of $1/3$ even below the critical points. The relative difference between $\mathcal{R}_{95}$ and $\mathcal{R}$ exceeds 60% for the least compact stars and is about 40% for the most compact stars. However, as mentioned previously, the fact of $M > \mathcal{R}/3$ may not indicate the formation of the photon sphere, because $\mathcal{R}$ covers only a part of the region
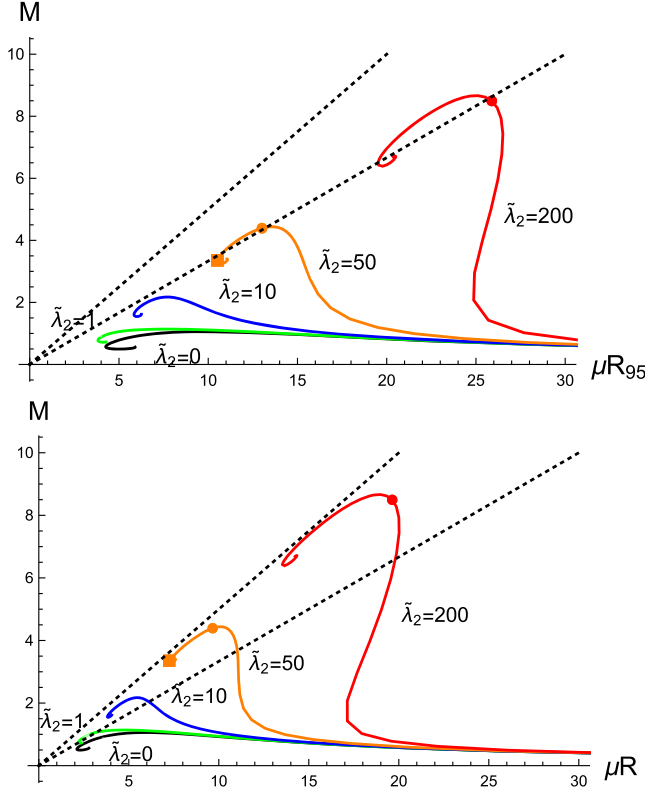
FIG. 6. M is shown as the function of $\mu\mathcal{R}_{95}$ (top) and $\mu\mathcal{R}$ (bottom) for $\tilde{\lambda}_2 = 0$ (black), 1 (green), 10 (blue), 50 (orange), and 200 (red). The dotted lines from the top represent those with the tilts $1/2$ and $1/3$, respectively. M is shown in the units of $8\pi M_{\mathrm{Pl}}^2/\mu$.

where the Proca field is localized, and should not be interpreted as an astrophysical surface of the star.

The difficulty for the formation of a photon sphere has also been observed in the case of scalar boson stars [52–54]. For instance, in the presence of the quartic-order self-interaction, the complex scalar field $V_\Phi = \frac{\mu_\Phi^2}{2}\bar{\Phi}\Phi + \frac{\lambda_\Phi}{4}(\bar{\Phi}\Phi)^2$ [see Eq. (2.1)], and the maximal value of $M/\mathcal{R}_{\mathrm{eff}}$ for scalar boson stars with $\lambda_\Phi > 0$ is about 0.16, while $M/\mathcal{R}_{\mathrm{eff}}$ for stars without the self-interaction $\lambda_\Phi = 0$ is about 0.08, both of which are much below $1/3$ [52,53]. In Refs. [52,53], $\mathcal{R}_{99}$ analogous to $\mathcal{R}_{95}$ [see Eq. (3.21)] was employed as an effective radius $\mathcal{R}_{\mathrm{eff}}$. Note that in our case $\mathcal{R}_{99}/\mathcal{R}_{95}$ for the Proca star solutions on the verge of the onset of a ghost instability is at most 1.10 for $\tilde{\lambda}_2 \approx 20$ and decreases as λ_2 increases, so $\mathcal{R}_{95}$ differs only a little from $\mathcal{R}_{99}$ for highly compact stars of interest. For the scalar potential $V_\Phi = \mu^2|\Phi|^2(1 - 2|\Phi|^2/\sigma_0^2)^2$ with the sextic-order power of $|\Phi|$, where σ_0 is a constant, the scalar field has a very sharp profile, and this self-interaction allows us to realize the maximal value of $M/\mathcal{R}_{\mathrm{eff}}$ close to $1/3$ [54]. Thus, in the case of scalar boson stars, although there is no ghost instability, the quartic-order self-interaction is not strong enough to support highly compact boson stars.

On the other hand, in the case of Proca stars, the quartic-order self-interaction (2.6) with Eq. (3.24) is strong enough to compress a Proca star. However, the onset of a ghost instability indicates that when one performs a numerical simulation of a collapse of a complex Proca field or a collision of two less compact Proca stars, numerical evolution would break down before the formation of a highly compact single Proca star in the context of EFT, as in other problems with a self-interacting Proca field [37–39]. Thus, unlike the case of scalar boson stars, the formation of a photon sphere is prevented because of the breakdown of the time evolution of the Proca field. It would be interesting to investigate whether the problem of a ghost instability could be cured by an inclusion of appropriate UV physics as discussed [36] (see also Ref. [55]).

Beyond the staticity and spherical symmetry, it is known that stationary and axisymmetric Proca stars without self-interactions can be compact enough to have a light ring in the stable branch (see, e.g., Refs. [56–58]). It would be also interesting to explore rotating Proca star solutions in our theory (2.8) with Eq. (2.6) and investigate whether the ghost instability would prevent the formation of the photon surface. For now, we leave these subjects for future studies.

V. CONCLUSIONS

In this paper, we have investigated the properties of Proca star solutions in the Einstein-complex Proca theory with quartic order self-interaction $\lambda_2[\bar{A}^\mu\bar{A}_\mu A^\nu A_\nu - (A^\mu\bar{A}_\mu)^2]$, in addition to the mass term $\mu^2 A^\mu\bar{A}_\mu$, where λ_2 represents the dimensionless coupling constant. Section II was devoted to introducing our theory from the comparison with the scalar-tensor theories. This type of the quartic-order self-interaction is different from $\lambda_1(A^\mu\bar{A}_\mu)^2$ previously considered, where λ_1 also represents the dimensionless coupling constant, and absent in the case of the real Proca field $\bar{A}_\mu = A_\mu$. The coupling constants λ_1 and λ_2 have to be negative if the complex Proca theory has a standard UV completion, e.g., the Higgs mechanism. However, a positive λ_1 or λ_2 cannot be excluded in the gravitational setup (or if getting rid of one of the fundamental assumptions), although its UV completion is not known. In the present paper, we take a bottom-up approach and discuss the phenomenological consequences of the new self-interaction λ_2 with both positive and negative values.

In Sec. III, we derived a closed set of the equations to determine the profile of Proca star solutions numerically. These equations are of the first-order differential equations with respect to the radial coordinate r. By solving them in the vicinity of the center $r = 0$, the boundary conditions were obtained. For an appropriate choice of the frequency of the complex Proca field, we constructed Proca star solutions numerically where the components of the Proca field are exponentially suppressed while the metric variables exponentially approach constant in the large distance

regions. We focused on the ground state solutions where the temporal and radial profiles of a complex Proca field have one and zero nodes, respectively. As in the case of Proca star solutions with other potentials, there are two conserved quantities which characterize Proca star solutions. One is the ADM mass M which can be read from the asymptotic value of the mass function, and the other is the Noether charge Q associated with the global $U(1)$ symmetry. We also derived the effective metric for the propagation of the perturbation of the self-interacting Proca field on top of a nontrivial Proca star background. If the temporal and radial components of the effective metric vanish, a Proca star solution suffers from ghost and gradient instabilities, respectively. The analysis of the effective metric indicated that in the case $\lambda_2 < 0$ a Proca star solution could suffer from a gradient instability, while in the case $\lambda_2 > 0$, it could suffer from a ghost instability.

Section IV was devoted to discussing the properties of the Proca star solutions. For simplicity, we set $\lambda_1 = 0$ and focused on the case $\lambda_2 \neq 0$. The second type of the interaction is absent in the limit of the real Proca field and has not been explored in the context of the Proca star. See Refs. [22–24] for the studies about the first type of the self-interactions. In the case of $\lambda_2 < 0$, we found that the ADM mass and Noether charge are always suppressed compared to those in the case of the massive Proca theory. The role of $\lambda_2 < 0$ is qualitatively similar to the coupling $\lambda_1 < 0$. In both cases, a gradient instability occurs for a sufficiently large amplitude of the Proca field. On the other hand, the properties of Proca stars for $\lambda_2 > 0$ are quite different from those for $\lambda_2 < 0$ (and those for $\lambda_1 > 0$, $\lambda_2 = 0$). For $\lambda_2 > 0$, the ADM mass and Noether charge are much more enhanced than those in the case of the purely massive Proca theory, and the relative difference between them is significantly larger. However, Proca star solutions with large compactness $M/\mathcal{R}_{95} \gtrsim 1/3$ suffer from a ghost instability at a finite radius. Although for $\lambda_2 > 0$ Proca stars could also be significantly more compact than those in the conventional case of the massive Proca theory, we have found that the onset of a ghost instability practically forbids the formation of the photon sphere or requires a knowledge of the UV completion. Although we did not explicitly discuss the most general case of $(\lambda_1 \neq 0, \lambda_2 \neq 0)$ in the main text, we numerically investigated several examples and found that turning on both couplings does not give novel features of the Proca stars. However, as we have not extensively studied all the parameter space, there might be an exceptional case which we leave for a future study.

In summary, if the Proca field is UV completed in a standard way $(\lambda_1 < 0, \lambda_2 < 0)$, both self-interactions make Proca stars less compact than those without self-interactions. On the other hand, the positive coupling constant $\lambda_2 > 0$ leads to compact Proca stars, which would be phenomenologically more interesting. The properties of the Proca stars with $\lambda_2 > 0$ are qualitatively different from

those of the conventional boson stars. It would be also remarkable that a ghost appears when the compactness exceeds $M/\mathcal{R}_{95} \simeq 1/3$, preventing the formation of a photon sphere in the regime of EFT.

It would be intriguing to see whether the pathology result of the formation of the photon sphere is generic in Proca stars. One may investigate Proca star solutions in Einstein-complex Proca theories including higher-order powers of $Z(= A^\mu A^\nu \bar{A}_\mu \bar{A}_\nu)$ as well as $Y(= \bar{A}^\mu A_\mu)$ [see Eqs. (2.4) and (2.5)]. At any order power of A_μ and $\bar{A}_\mu$, the self-interacting potential can be constructed by a linear combination of powers of Y and Z. For instance, the most general sextic-order self-interacting potential is a linear combination of Y^3 and YZ, and the most general octic-order one is that of Y^4, Y^2Z, and Z^2. The higher-order interactions become important for a sufficiently large Proca amplitude and may influence the properties of highly compact Proca stars. It would be interesting to explore the possibility of having a highly compact star before the onset of pathological instability thanks to the higher-order interactions. It is also important to see whether the pathology can be cured by appropriate UV physics as the ghost or gradient instability is expected to appear generically in the self-interacting Proca field.

APPENDIX: POSITIVITY BOUNDS ON SPIN-1 FIELDS

The positivity bounds are S-matrix constraints on the EFT to admit unitary, Poincaré invariant, causal, and local UV completion [44]. Let us consider an $s \leftrightarrow u$ symmetric scattering amplitude $\mathcal{M}(s, t)$ of a nongravitational process $XY \rightarrow XY$ with fixed t where $\{s, t, u\}$ are the Mandelstam variables. The $s \leftrightarrow u$ crossing symmetry is manifest for a scattering of spin-0 particles, while special care is needed for spin-1 particles (and generic spinning particles) [59,60]. However, in the forward limit $t \rightarrow 0$, which we shall focus on in the following, one can derive the positivity bounds for spin-1 particles similarly to spin-0 particles by working with linear polarizations [59]. The mentioned properties lead to the so-called twice-subtracted dispersion relation which relates the amplitude with the integral of the imaginary part of the amplitude (and polynomial terms).

In particular, the s^2 coefficient of the amplitude at $s = \mu_X^2 + \mu_Y^2$ satisfies

$$\frac{1}{2}\frac{d^2\mathcal{M}(s,0)}{ds^2}\bigg|_{s=\mu_X^2+\mu_Y^2} = \frac{1}{\pi}\int_{\text{cut}}ds'\frac{\text{Im}\mathcal{M}(s',0)}{(s'-\mu_X^2-\mu_Y^2)^3} \quad (A1)$$

in the forward limit $t \to 0$, where the integral runs along the branch cut (and poles on the real axis if any) and μ_X and μ_Y are the masses of X and Y, respectively. The left-hand side of (A1) is evaluated at low energy and can be therefore computed by the EFT. The right-hand side involves the integral in the high-energy region and cannot be explicitly computed unless UV completion is given. However, unitarity ensures the imaginary part of the forward limit amplitude is positive, leading to the bound

$$\frac{1}{2}\frac{d^2\mathcal{M}(s,0)}{ds^2}\bigg|_{s=\mu_X^2+\mu_Y^2} > 0. \quad (A2)$$

Therefore, the s^2 coefficient of the EFT amplitude has to be positive, which is known as the positivity bound.

When we decompose the complex Proca field into the real and imaginary parts, $A_\mu = A_\mu^1 + iA_\mu^2$, the Proca field Lagrangian (2.3) is given by

$$\mathcal{L} = \sum_{a=1}^{2}\left[-\frac{1}{4}F^{a\mu\nu}F_{\mu\nu}^a - \frac{\mu^2}{2}A^{a\mu}A_\mu^a\right]$$
$$-\frac{\lambda_1}{4}(A^{1\mu}A_\mu^1 + A^{2\mu}A_\mu^2)^2$$
$$-\lambda_2[(A^{1\mu}A_\mu^2)^2 - A^{1\mu}A_\mu^1 A^{2\mu}A_\mu^2]. \quad (A3)$$

The linear polarization basis of the spin-1 particle for the four-momentum $p^\mu = (p^0, 0, 0, p^3)$ is given by

$$\epsilon_\mu^{T_1} = (0,1,0,0), \qquad \epsilon_\mu^{T_2} = (0,0,1,0),$$
$$\epsilon_\mu^L = \frac{1}{\mu}(p^3,0,0,p^0), \quad (A4)$$

where $\epsilon_\mu^{T_1}, \epsilon_\mu^{T_2}$ are the basis for transverse modes, while ϵ_μ^L is the basis for longitudinal mode. Since the interactions that we are considering do not involve derivatives, the scatterings of the transverse modes do not lead to the $s^2 = \mathcal{O}(p^4)$ term at the tree level. The s^2 coefficient arises from the interaction $(A^{a\mu}A_\mu^b)^2$ in the scattering $ab \to ab$ of the longitudinal modes where $a, b = 1, 2$. The coupling constants λ_1 and λ_2 are only relevant to $a = b$ and $a \neq b$, respectively. We thus find the inequalities (2.7) by applying the bound (A2) to the processes $aa \to aa$ and $ab \to ab (a \neq b)$ in the Proca field Lagrangian (2.3).

The extension of the positivity bounds to gravitational theories is not straightforward. The main difficulty arises from the presence of the s^2/t term due to the graviton t-channel exchange which gives a singular contribution in the forward limit. The singular contribution is canceled under the assumption that the amplitudes exhibit an appropriate high-energy behavior as predicted by string theory, and then the gravitational positivity bounds can be derived [47]. However, the bounds contain an uncertainty of the order of M_{Pl}^{-2} due to the lack of precise knowledge of quantum gravity. A small violation of the nongravitational positivity bound (A2) could be possible in the gravitational system (see also Refs. [45,46,48–51] for related discussions). Allowing the small violation, the gravitational positivity bounds read

$$\lambda_1, \lambda_2 < \mathcal{O}(1) \times \frac{\mu^4}{M_{\text{Pl}}^2 M^2} \quad (A5)$$

in the Einstein-Proca theory (2.8), where M is a scale depending on the details of the high-energy behavior of the amplitude. If the scale M is given by the IR physics $M = \mathcal{O}(\mu)$, the coupling constants λ_1, λ_2 can take sufficiently large positive values to affect properties of Proca stars. On the other hand, the positive values are practically forbidden if M is related to a UV physics scale, e.g., the cutoff scale of the EFT or the quantum gravity scale.

[1] T. Clifton, P. G. Ferreira, A. Padilla, and C. Skordis, Modified gravity and cosmology, Phys. Rep. **513**, 1 (2012).

[2] C. M. Will, The confrontation between general relativity and experiment, Living Rev. Relativity **17**, 4 (2014).

[3] E. Berti, K. Yagi, and N. Yunes, Extreme gravity tests with gravitational waves from compact binary coalescences: (I) inspiral-merger, Gen. Relativ. Gravit. **50**, 46 (2018).

[4] E. Berti, K. Yagi, H. Yang, and N. Yunes, Extreme gravity tests with gravitational waves from compact binary coalescences: (II) ringdown, Gen. Relativ. Gravit. **50**, 49 (2018).

[5] L. Barack et al., Black holes, gravitational waves and fundamental physics: A roadmap, Classical Quantum Gravity **36**, 143001 (2019).

[6] V. Cardoso and P. Pani, Tests for the existence of black holes through gravitational wave echoes, Nat. Astron. **1**, 586 (2017).

[7] V. Cardoso and P. Pani, Testing the nature of dark compact objects: A status report, Living Rev. Relativity **22**, 4 (2019).

[8] P. Jetzer, Boson stars, Phys. Rep. **220**, 163 (1992).

[9] F. E. Schunck and E. W. Mielke, General relativistic boson stars, Classical Quantum Gravity **20**, R301 (2003).

[10] L. Visinelli, Boson stars and oscillatons: A review, Int. J. Mod. Phys. D **30**, 2130006 (2021).

[11] S. L. Liebling and C. Palenzuela, Dynamical boson stars, Living Rev. Relativity **15**, 6 (2012).

[12] D. J. Kaup, Klein-Gordon geon, Phys. Rev. **172**, 1331 (1968).

[13] R. Ruffini and S. Bonazzola, Systems of selfgravitating particles in general relativity and the concept of an equation of state, Phys. Rev. **187**, 1767 (1969).

[14] R. Friedberg, T. D. Lee, and Y. Pang, Mini—soliton stars, Phys. Rev. D **35**, 3640 (1987).

[15] M. Gleiser, Stability of boson stars, Phys. Rev. D **38**, 2376 (1988).

[16] M. Gleiser and R. Watkins, Gravitational stability of scalar matter, Nucl. Phys. **B319**, 733 (1989).

[17] S. H. Hawley and M. W. Choptuik, Boson stars driven to the brink of black hole formation, Phys. Rev. D **62**, 104024 (2000).

[18] D. Guerra, C. F. B. Macedo, and P. Pani, Axion boson stars, J. Cosmol. Astropart. Phys. 09 (2019) 061.

[19] R. Brito, V. Cardoso, C. A. R. Herdeiro, and E. Radu, Proca stars: Gravitating Bose–Einstein condensates of massive spin 1 particles, Phys. Lett. B **752**, 291 (2016).

[20] Y. Brihaye, T. Delplace, and Y. Verbin, Proca Q balls and their coupling to gravity, Phys. Rev. D **96**, 024057 (2017).

[21] I. S. Landea and F. Garcia, Charged Proca stars, Phys. Rev. D **94**, 104006 (2016).

[22] M. Minamitsuji, Vector boson star solutions with a quartic order self-interaction, Phys. Rev. D **97**, 104023 (2018).

[23] C. A. R. Herdeiro and E. Radu, Asymptotically flat, spherical, self-interacting scalar, Dirac and Proca stars, Symmetry **12** (2020) 2032.

[24] V. Cardoso, C. F. B. Macedo, K.-i. Maeda, and H. Okawa, ECO-spotting: Looking for extremely compact objects with bosonic fields, Classical Quantum Gravity **39**, 034001 (2022).

[25] H.-Y. Zhang, M. Jain, and M. A. Amin, Polarized vector oscillons, Phys. Rev. D **105**, 096037 (2022).

[26] M. Jain, Soliton stars in Yang-Mills-Higgs theories, Phys. Rev. D **106**, 085011 (2022).

[27] K. Aoki, K.-i. Maeda, Y. Misonoh, and H. Okawa, Massive graviton geons, Phys. Rev. D **97**, 044005 (2018).

[28] R. Brito, S. Grillo, and P. Pani, Black Hole Superradiant Instability from Ultralight Spin-2 Fields, Phys. Rev. Lett. **124**, 211101 (2020).

[29] M. Jain and M. A. Amin, Polarized solitons in higher-spin wave dark matter, Phys. Rev. D **105**, 056019 (2022).

[30] N. Sanchis-Gual, C. Herdeiro, J. A. Font, E. Radu, and F. Di Giovanni, Head-on collisions and orbital mergers of Proca stars, Phys. Rev. D **99**, 024017 (2019).

[31] F. Di Giovanni, N. Sanchis-Gual, P. Cerdá-Durán, M. Zilhão, C. Herdeiro, J. A. Font, and E. Radu, Dynamical bar-mode instability in spinning bosonic stars, Phys. Rev. D **102**, 124009 (2020).

[32] J. C. Bustillo, N. Sanchis-Gual, A. Torres-Forné, J. A. Font, A. Vajpeyi, R. Smith, C. Herdeiro, E. Radu, and S. H. W. Leong, GW190521 as a Merger of Proca Stars: A Potential New Vector Boson of 8.7×10^{-13} eV, Phys. Rev. Lett. **126**, 081101 (2021).

[33] C. A. R. Herdeiro, A. M. Pombo, E. Radu, P. V. P. Cunha, and N. Sanchis-Gual, The imitation game: Proca stars that can mimic the Schwarzschild shadow, J. Cosmol. Astropart. Phys. 04 (2021) 051.

[34] J. a. L. Rosa and D. Rubiera-Garcia, Shadows of boson and Proca stars with thin accretion disks, Phys. Rev. D **106**, 084004 (2022).

[35] J. a. L. Rosa, P. Garcia, F. H. Vincent, and V. Cardoso, Observational signatures of hot spots orbiting horizonless objects, Phys. Rev. D **106**, 044031 (2022).

[36] K. Aoki and M. Minamitsuji, Resolving the pathologies of self-interacting Proca fields: A case study of Proca stars, Phys. Rev. D **106**, 084022 (2022).

[37] K. Clough, T. Helfer, H. Witek, and E. Berti, Ghost Instabilities in Self-Interacting Vector Fields: The Problem with Proca Fields, Phys. Rev. Lett. **129**, 151102 (2022).

[38] A. Coates and F. M. Ramazanoğlu, Intrinsic Pathology of Self-Interacting Vector Fields, Phys. Rev. Lett. **129**, 151103 (2022).

[39] Z.-G. Mou and H.-Y. Zhang, Singularity Problem for Interacting Massive Vectors, Phys. Rev. Lett. **129**, 151101 (2022).

[40] A. Coates and F. M. Ramazanoğlu, Coordinate Singularities of Self-Interacting Vector Field Theories, Phys. Rev. Lett. **130**, 021401 (2023).

[41] H. Fukuda and K. Nakayama, Aspects of nonlinear effect on black hole superradiance, J. High Energy Phys. 01 (2020) 128.

[42] W. E. East, Vortex String Formation in Black Hole Superradiance of a Dark Photon with the Higgs Mechanism, Phys. Rev. Lett. **129**, 141103 (2022).

[43] C. Herdeiro, E. Radu, and E. dos Santos Costa Filho, Proca-Higgs balls and stars in a UV completion for Proca self-interactions, arXiv:2301.04172.

[44] A. Adams, N. Arkani-Hamed, S. Dubovsky, A. Nicolis, and R. Rattazzi, Causality, analyticity and an IR obstruction to UV completion, J. High Energy Phys. 10 (2006) 014.

[45] Y. Hamada, T. Noumi, and G. Shiu, Weak Gravity Conjecture from Unitarity and Causality, Phys. Rev. Lett. **123**, 051601 (2019).

[46] L. Alberte, C. de Rham, S. Jaitly, and A. J. Tolley, Positivity bounds and the massless spin-2 pole, Phys. Rev. D **102**, 125023 (2020).

[47] J. Tokuda, K. Aoki, and S. Hirano, Gravitational positivity bounds, J. High Energy Phys. 11 (2020) 054.

[48] M. Herrero-Valea, R. Santos-Garcia, and A. Tokareva, Massless positivity in graviton exchange, Phys. Rev. D **104**, 085022 (2021).

[49] S. Caron-Huot, D. Mazac, L. Rastelli, and D. Simmons-Duffin, Sharp boundaries for the swampland, J. High Energy Phys. 07 (2021) 110.

[50] L. Alberte, C. de Rham, S. Jaitly, and A. J. Tolley, Reverse Bootstrapping: IR Lessons for UV Physics, Phys. Rev. Lett. **128**, 051602 (2022).

[51] M. Herrero-Valea, A. S. Koshelev, and A. Tokareva, UV graviton scattering and positivity bounds from IR dispersion relations, Phys. Rev. D **106**, 105002 (2022).

[52] P. Amaro-Seoane, J. Barranco, A. Bernal, and L. Rezzolla, Constraining scalar fields with stellar kinematics and collisional dark matter, J. Cosmol. Astropart. Phys. 11 (2010) 002.

[53] G. F. Giudice, M. McCullough, and A. Urbano, Hunting for dark particles with gravitational waves, J. Cosmol. Astropart. Phys. 10 (2016) 001.

[54] V. Cardoso, S. Hopper, C. F. B. Macedo, C. Palenzuela, and P. Pani, Gravitational-wave signatures of exotic compact objects and of quantum corrections at the horizon scale, Phys. Rev. D **94**, 084031 (2016).

[55] E. Barausse, M. Bezares, M. Crisostomi, and G. Lara, The well-posedness of the Cauchy problem for self-interacting vector fields, J. Cosmol. Astropart. Phys. 11 (2022) 050.

[56] P. V. P. Cunha, C. Herdeiro, E. Radu, and N. Sanchis-Gual, The fate of the light-ring instability, arXiv:2207.13713.

[57] N. Sanchis-Gual, J. Calderón Bustillo, C. Herdeiro, E. Radu, J. A. Font, S. H. W. Leong, and A. Torres-Forné, Impact of the wavelike nature of Proca stars on their gravitational-wave emission, Phys. Rev. D **106**, 124011 (2022).

[58] I. Sengo, P. V. P. Cunha, C. A. R. Herdeiro, and E. Radu, Kerr black holes with synchronised Proca hair: Lensing, shadows and EHT constraints, J. Cosmol. Astropart. Phys. 01 (2023) 047.

[59] B. Bellazzini, Softness and amplitudes' positivity for spinning particles, J. High Energy Phys. 02 (2017) 034.

[60] C. de Rham, S. Melville, A. J. Tolley, and S.-Y. Zhou, UV complete me: Positivity bounds for particles with spin, J. High Energy Phys. 03 (2018) 011.